# Delft University of Technology

Residual ultimate strength of seamless metallic pipelines under a bending moment-a numerical investigation

Cai, Jie; Jiang, Xiaoli; Lodewijks, Gabriel; Pei, Zhiyong; Wu, Weiguo

**Important note**
To cite this publication, please use the final published version (if applicable).
Please check the document version above.

# Residual ultimate strength of seamless metallic pipelines under a bending moment-a numerical investigation

Jie Cai[a,*], Xiaoli Jiang[a], Gabriel Lodewijks[b], Zhiyong Pei[c], Weiguo Wu[c]

[a] Department of Maritime and Transport Technology, Delft University of Technology, 2628 CD Delft, The Netherlands
[b] School of Aviation, University of New South Wales, NSW 2052, Sydney, Australia
[c] Departments of Naval Architecture, Ocean and Structural Engineering, School of Transportation, Wuhan University of Technology, PR China

ABSTRACT

Numerical investigation is conducted in this paper on both intact and dented seamless metallic pipelines (diameter-to-thickness ratio $D/t$ around 21), deploying nonlinear finite element method (FEM). A full numerical model is developed, capable of predicting the residual ultimate strength of pipes in terms of bending capacity ($M_{cr}$) and critical curvature ($\kappa_{cr}$). The simulation results are validated through test results by using the measured material properties and specimen geometry. An extensive parametric investigation is conducted on the influences of material anisotropy, initial imperfection, friction of the test set-up and dent parameters. It is found that the structural response is quite sensitive to the frictions that have been introduced by the test configuration. For a pipe with a considerable dent size, the effect of manufacturing induced initial imperfection is insignificant and can be neglected in the FEM simulation. The material yield stress in the pipe longitudinal direction dominates the bending capacity of structures. In the end, formulas are proposed to predict the residual ultimate strength of dented metallic pipes under pure bending moment, which can be used for practical purposes. A satisfying fit is obtained through the comparison between the formulas and FEM methods.

## 1. Introduction

In previous work of Cai et al. (2017b), an experimental investigation on the bending capacity of the damaged seamless metallic pipelines has been completed. Artificial damage such as a dent, metal loss, a crack and their combinations thereof is properly introduced on specimens. Meanwhile, an initial numerical investigation on the dented pipes has been performed based on a simplified FEM model from the former research of the authors Cai et al. (2018a). However, some influential factors such as the real boundary effect, and the frictions from the test configuration have not been accounted for due to simplifications. As one of the numerical investigation series, the present research focus on both the intact and the dented pipes in order to compare with test and further quantify the dent effect.

In pipelines, structural damage cannot be avoided during their entire life time, which may compromise the structural safety and leads to large loss of assets (Ghaednia et al., 2015; Cai et al., 2017a). It is estimated by PHMSA (2017) that about 23% of all the reported structural damage on pipelines in US in the past 20 years was caused by mechanical interference. Scenarios in practice such as dropping of foreign objects, fishing equipment impact, dragging anchors under water and

sinking vessels (Bjørnøy et al., 2000; Macdonald and Cosham, 2005; DNV, 2010) can probably introduce large dent damage to pipes so that the residual ultimate strength of structure may be considerably affected. As simply stated in the rule of DNV (2013a,b), the maximum accepted permanent dent depth due to impact accident should not be larger than 0.05D in a low impact frequency.

Considerable research on the ultimate strength behavior of pipes without structural damage subjected to bending moment has been conducted in the past (Jones and Kitching, 1966; Weiner and Smith, 1976; Sherman, 1976; Gellin, 1980; Murphey and Langner, 1985). During the last twenty years, Bai et al. (1994) proposed prediction equations of ultimate limit states of intact pipes with $D/t$ ratios from 10 to 40 based on an existing experimental database. Gresnigt and Van Foeken (2001) discussed the governing parameters such as geometrical deviations and material properties on pipes with $D/t$ from 22 to 45. It was highlighted that the manufacturing methods had considerable influences on the governing parameters and the pipe local buckling resistance. Experimentally, Es et al. (2016) extensively investigated the ultimate structural behaviors of pipes without structural damage subjected to bending moment, deploying a spiral-welded steel tubes with 42-inch-diameter and $D/t$ between 65 and 120. Based on the test

---

| Nomenclature | | $D$ | outer diameter of pipe [mm] |
|---|---|---|---|
| | | $d_d$ | dent depth [mm] |
| $\kappa_0$ | the referential curvature of pipe [1/m] | $L$ | full length of specimen [mm] |
| $\kappa_i$ | critical curvature of intact pipe (either from test or simulation) [1/m] | $L1$ | half length of specimen under pure bending [mm] |
| | | $L2/L4$ | length of the loading/support strip [mm] |
| $\kappa_{cr}$ | critical curvature of pipe [1/m] | $L3$ | original bending arm [mm] |
| $\lambda_l$ | normalized dent length | $L5$ | side length of specimen [mm] |
| $\lambda_w$ | normalized dent width | $l_d$ | dent length [mm] |
| $\lambda_{cl}$ | critical half-wavelength | $M_i$ | ultimate bending moment of intact pipe (either from test or simulation) [kNm] |
| $\omega$ | dent depth variation [mm] | | |
| $\sigma_y$ | material yield stress [MPa] | $M_y$ | plastic bending moment [kNm] |
| $\sigma_h$ | material yield stress in the pipe hoop direction [MPa] | $M_{cr}$ | residual ultimate bending moment |
| $\theta_d$ | dent angle [deg] | $R$ | pipe outer radius [mm] |
| $\varepsilon_{11}$ | strain component in pipe axial direction | $t$ | pipe thickness [mm] |
| $\varepsilon_{22}$ | strain component in pipe hoop direction | $w_d$ | dent width [mm] |

results, Vasilikis et al. (2016) conducted a consecutive numerical investigation. The effect of spiral-welded manufacturing method has been described in detail. Other relevant research can be seen from literature (Vitali et al., 2005; Guarracino et al., 2009; Hilberink, 2011; Bai and Bai, 2014a; b). Nevertheless, the investigations on the residual ultimate strength of damaged metallic pipes subjected to bending moment are relatively rare. The majority of the research on damaged pipes concentrated on the bursting of pipe subjected to internal pressure or collapse capacity subjected to external pressure, such as Park and Kyriakides (1996) and Bjørnøy et al. (2000).

Therefore, in the present research, on the basis of both the experimental investigation and the former research of the dented pipes, the simulations of intact seamless metallic pipes and pipes with artificial dent are conducted in order to compare with test and further quantify the dent effect on pipes under pure bending moment. The full numerical models are developed, capable of accounting for the variation of possible parameters such as material, geometrical nonlinearality, damage type and damage size in an efficient way. The nonlinear finite element method (FEM) is deployed for the simulation.

The structure of this paper is arranged as follows. In Section 2, the test set-up and the specimens that are deployed are briefly reviewed. Section 3 comprehensively describes the developed full numerical models for simulation of different types of specimens, including intact model without damage and the dented model. Furthermore, the numerical predictions are validated by the test results in terms of structural failure modes, strain variation, and bending moment-curvature diagrams in Section 4. In Section 5, a parametric investigation is performed, accounting for the influential parameters such as material anisotropy, initial imperfection and friction of the set-up that have been observed in the physical test. Afterwards, the effects of dent parameters including dent depth, length and width are analyzed and discussed in Section 6. Empirical formulas are then proposed to predict the residual ultimate strength of metallic pipes under bending moment. Finally, this paper ends with some concluding remarks.

## 2. Tests and specimens overview

In this section, the set-up of four-point bending tests and specimens are briefly reviewed. The details of the pipe test have been presented in the relevant experimental investigation part of Cai et al. (2017b).

Fig. 1 shows the designed four-point bending test set-up. The principal dimensions and specific geometrical distribution of specimens are listed in Table 1. During the physical test, 39 seamless specimens in terms of both intact and the ones with artificial damage on their surface were used. The $D/t$ ratio of the specimens varied around 21 due to the manufacturing deviation. The deployed specimen material is Q345B (GB/T 1591, 2008), which is a typical material for transmission pipes with a minimum yield stress of 345 MPa.

Four specimens are intact with no structural damage, whereas 35 specimens are intentionally damaged through carefully designed test in the laboratory. All the structural damage is introduced properly on each specimen before the strength test, located at the center of specimen either on the compression side or on the tensile side. The test data are measured and documented extensively. In this paper, only the type of dent structural damage, as shown in Fig. 2, has been accounted for. Other types of damage have been investigated separately by the authors Cai et al. (2018b, c). As seen in Fig. 3, the dent is introduced by a quasi-static indentation with different types of indenters. In this paper, the dent on specimens is produced by the indenter with an arc-shape.

The specimens that will be deployed for the following validation are categorized into two groups (all the series numbers of specimens in this paper are exactly the same with the ones in the experimental investigation of Cai et al. (2017b)): (a) specimens within the first group without artificial structural damage, including S1N1, S1N2, S1N3 and S1N4; (b) dented specimens within the second group with dent in different dent angle and size, including S2N1, S2N2, S2N3 and S2N5.
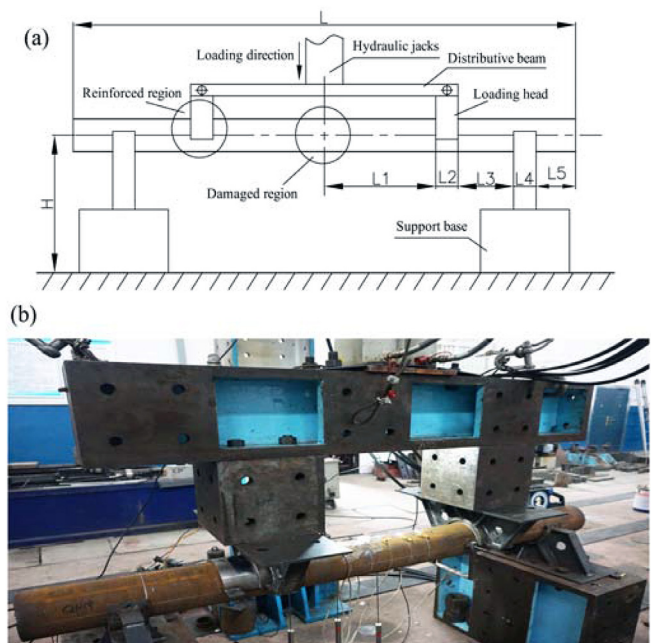


**Fig. 1.** The configuration of four-point bending test: (a) the sketch of test set-up; (b) the real test set-up in laboratory.

**Table 1**
The geometrical distribution of specimens for four-point bending test.

| Parameters | Value |
|---|---|
| Full length of specimen (L) (mm) | 2200 |
| Half length under pure bending (L1) (mm) | 400 |
| Length of loading\support strip (L2 \ L4) (mm) | 100 |
| Length of original bending arm (L3) (mm) | 300 |
| Side length (L5) (mm) | 200 |
| Specimen type | Seamless (hot-rolled) |
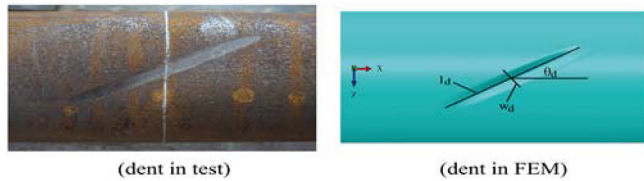


**Fig. 2.** The schema of dent damage on both test specimen and numerical model ($\theta_d = 45^o$, $l_d$: dent length, $w_d$: dent width).
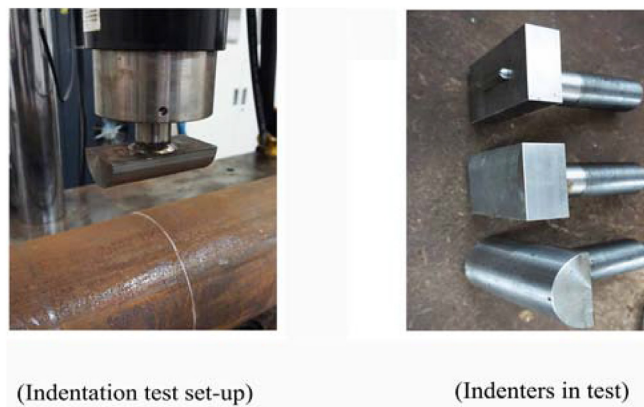


**Fig. 3.** The indentation test set-up and the used indenters in the test.

## 3. Finite element models

The numerical models have been developed in ABAQUS/Standard (Abaqus6.13, 2013) through python for the simulation of test specimens and the investigation of parameters effects. Symmetry has been introduced in the models of intact specimen for the sake of simulation efficiency, whereas full models have been deployed for the damaged specimens to avoid the possible boundary effect on damage. A strip that is used to mimic the loading head and support base from test is introduced for both the loading and the supporting of the specimens in numerical predictions, as illustrated in Fig. 4. A friction coefficient of 0.26, as estimated in engineering practice for steel, is deployed for the contact between specimen and strips. Moreover, a surface-to-surface contact strategy with finite sliding is used during simulation. In this way, the bending moment has been produced through the two vertical downward forces, leading to the same four-point loading pattern as used in the physical test.

In order to avoid the pre-failure that is caused by the loading heads, the structures, other than the central bending parts, are reinforced by increasing of the wall thickness which is equivalent with the function of half-sleeves in the physical tests. Furthermore, the initial imperfection in terms of a wave-type is introduced for all the models in the form of the combination of the first two orders of the eigenvalue buckling modes. The imperfection amplitude is set to $3\%t$ (t is the pipe thickness) based on the recommendation from Es et al. (2016) due to the lack of data in current test, as seen in Fig. 5.

An elastic-plastic material with von Mises yield criterion and isotropic hardening is deployed. When the anisotropy characteristic in terms of different material yield stress between specimen hoop and longitudinal direction is accounted for, the Hill48 criterion (Hill, 1948) is deployed. For both intact and dented models, the cylindrical shells are modeled with a curved three-dimensional shell element (S8R5) which is a 8-node, quadrilateral element with reduced integration and five degrees of freedom in each node (three displacement components and two in-surface rotation components), providing an accurate and economical simulation. The discrete rigid element R3D4 (Abaqus6.13, 2013) is employed for the loading and support strips.

### 3.1. Intact model

For the intact model that does not contain any artificial damage, the symmetry and shell element are deployed as mentioned above. The entire model has been partitioned into four basic segments for different mesh strategy, as shown in Fig. 4 (a). In Segments 1 and 3, a relative dense mesh is assigned with the size of 4 mm in hoop direction and 3 mm in logitudinal direction, while a coarse mesh is assigned to Segments 2 and 4 with the largest size of 12 mm in logitudinal direction through a double-bias strategy. In other words, there are at least twenty-one elements within a half-wave length (expressed as $\lambda_{cl} = 1.728\sqrt{Rt}$ (Prabu et al., 2010)) of refined regions, while there are at least five elements within a half-wave length of the coarse regions. An overall of 100000 elements for each model is therefore produced. A displacement-control strategy with a maximum of 0.001 mm downward displacement in each increment is deployed for loading so that every detail variation of the structural behavior of specimens can be traced. A central reference point that is coupled with the corresponding cross-section has been employed for the symmetrical boundary condition through the kinematic coupling method. Material type L7 from the test of Cai et al. (2017b) is deployed for all the specimens, with the yield stress of 378 MPa, the ultimate tensile stress of 542 MPa and the maximum elongation of 24.6%. A slight anisotropy in terms of yield stress ratio of 1.063 ($\sigma_h/\sigma_y$) is set for the intact model due to the observation from material tensile test.

### 3.2. Dented model

On the basis of the numerical model of the intact pipe, the full model of specimen with dent is developed, accounting for the variation of dent angle and size, as seen in Fig. 6. Here, the dented region has not been specially partitioned as in the former research (Cai et al., 2018a), instead, a general refined mesh strategy is assigned in this region. The mesh is largely refined in the damaged region in order to avoid the artificial bending moment, with the minimum mesh equal to 2 mm, i.e. less than 3.2% of the half-wave length ($\lambda_{cl} = 1.728\sqrt{Rt}$) of cylindrical shells. The symmetry strategy has not be deployed any more due to the introducing of structural damage. An overall of 170000 elements for each dented model is therefore produced.

The shape of the dent is based on the physical test (see Figs. 2 and 3). An indenter with the arc-shape is used for the produce of the dent in
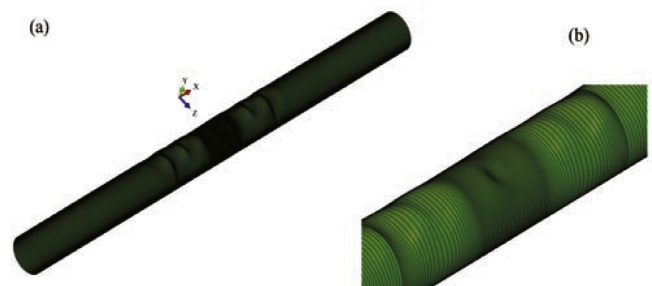


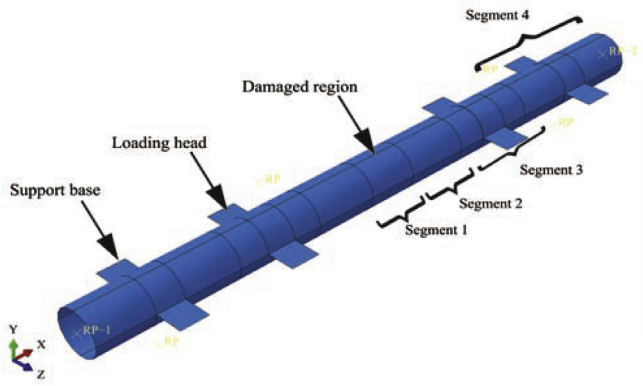**Fig. 4.** FEM model according to test set-up.

**Fig. 5.** (a) the initial imperfection in terms of wave-type on the pipe specimens (imperfection amplitude has been zoomed in for the sake of clarity); (b) the details of imperfection.
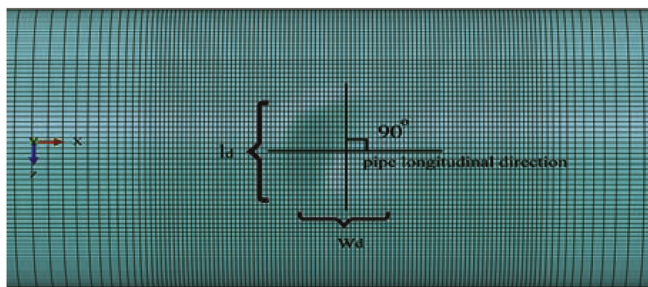


**Fig. 6.** Schema of mesh distribution of dented specimen and dent parameters ($\theta_d = 90^o$).

this paper. It is assumed that such physical shape is similar to the co-sinusoidal shape from original design, as expressed in Eq. (1). The impact-induced residual stress has not been taken into account in this paper. An initial exploration for such residual stress has been completed in the former research by Cai et al. (2016), which reflects that a little effect has been produced by such residual stress. The dent angle (the range of $\theta_d$ is between $0^o$ and $90^0$) is defined as the angle between the dent axis in its length direction and the pipe axis in the longitudinal direction, increasing in a clockwise direction, as illustrated in Figs. 2 and 6. Hence, a dent with angle of $90^o$ locates in the pipe hoop direction, while a dent with angle of $0^o$ locates in the pipe longitudinal direction. Dent parameters including length ($l_d$), width ($w_d$) and depth ($d_d$) are also defined.

$$\omega = d_d \cdot (1 + \cos(2\pi x/l_d)) \cdot (1 + \cos(2\pi y/w_d))/4 \qquad (1)$$

## 4. Simulation of experiments

In this section, the structural behavior of the specimens from experiments are simulated based on the developed numerical models in the previous section. The simulation results have been compared with the test data in terms of the structural failure modes, strain distributions and bending moment-curvature diagrams.

### 4.1. Reference values

The bending moment is generally normalized by the plastic bending moment $M_y = 4R^2 t\sigma_y$; Meanwhile, the bending curvature $\kappa$ is normalized by the curvature-like expression $\kappa_0 = t/4R^2$. It should be noted that only global curvature is selected for comparison between test and numerical simulation. The selected locations for calculation of the global curvature in simulation are exactly the same with tests, while the bending moment is the resultant of all the node forces multiplying their
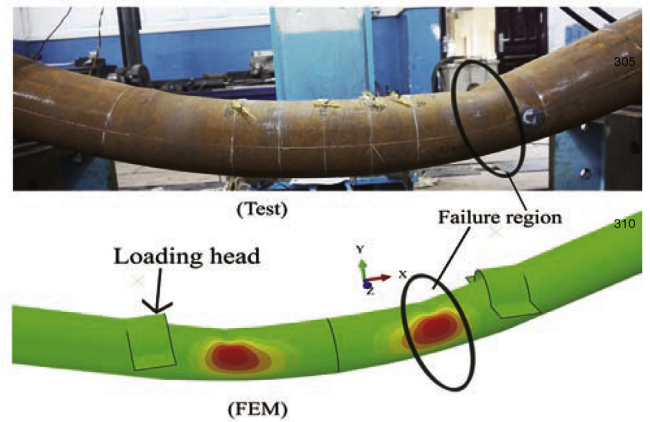


**Fig. 7.** The comparison of failure mode of intact specimen without damage (S1N4, the color distribution denotes the lateral displacement). (For interpretation of the references to color in this figure legend, the reader is referred to the Web version of this article.)

corresponding force arms in the central cross-section of the specimen. Moreover, for the proposed formulas of damaged pipes, the results from the intact pipes are used as the reference value, expressed as $M_i$ and $k_i$, respectively.

### 4.2. Structural failure modes

The comparison results of structural failure modes of specimens between numerical prediction and test are illustrated in Fig. 7 and Fig. 8. As a result of the increase of the structural deformation in the form of ovalization in the pipe cross-sections, the specimens fail due to the increasing of bending moment. The initiation of failure for an intact specimen happens on the top region far from the center of the specimen with an extra large ovalization in the same cross-section, as shown in Fig. 7, whereas the damaged specimen fails in the center of specimen due to the occurrence of dent, as seen in Fig. 8. All the failure modes are in the form of an inward bulge on the pipe top and an outward bulge on the pipe lateral sides. The occurrence of dent has produced a rapid increase of the ovalization in the dented cross-section, introducing a large concentration of the lateral displacement. The failure mode and failure location between the test and the simulation have a good agreement with each other.

Fig. 9 shows the evolution of axial strain ($\varepsilon_{11}$) along the pipe
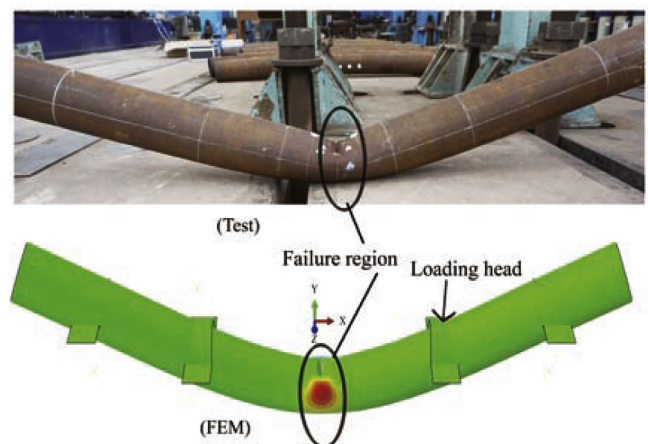


**Fig. 8.** The comparison of failure mode of specimen with dent damage (S2N2, the color distribution denotes the lateral displacement). (For interpretation of the references to color in this figure legend, the reader is referred to the Web version of this article.)
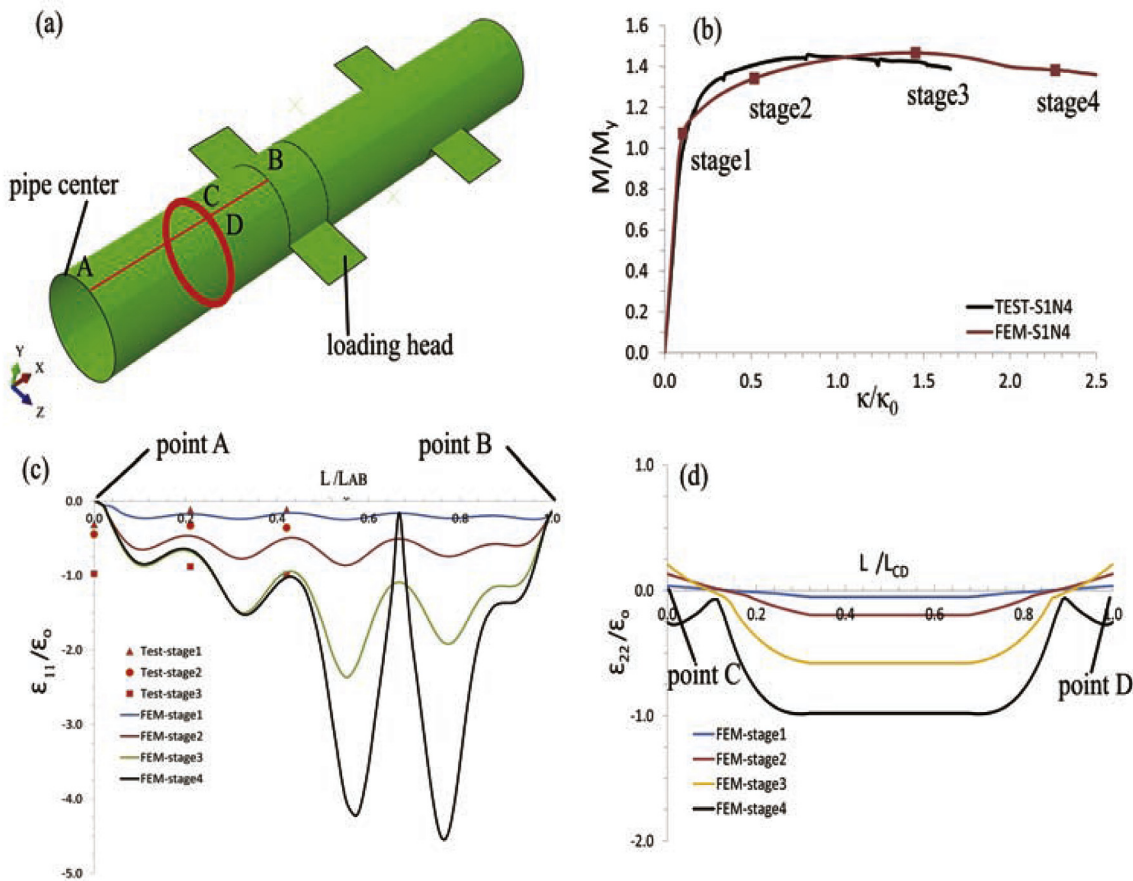
**Fig. 9.** (a) sketch of representative paths on specimen surface; (b) four stages during the loading of specimen S1N4; (c) strain along longitudinal path of pipe specimen (AB, S1N4); (d) strain along hoop path of specimen (CD, S1N4).

longitudinal path (*AB*) and the hoop strain ($\varepsilon_{22}$) along the pipe hoop path (*CD*) in four different loading stages of specimen S1N4, respectively. The test results from the measurement of strain gauges in specific points and corresponding stages (such as stage1, stage2, and stage3) are also presented, accompanying by the simulation results. Fig. 10 shows the corresponding locations for strain measurements on an intact specimen. Along the longitudinal direction of the specimen, including Point A (pipe center), 05D (∽ 0.21*AB*), and 1D (∽ 0.42*AB*), the strain gauges are put on the top side (compression side) of the pipe. Only axial strains are presented due to the lack of data. The numbers in this figure indicate the measured directions of the strain gauges. It is observed that the variation of $\varepsilon_{11}$ in the beginning is quite benign with a uniform distribution, whereas a large increase and localization of strain happen in the critical region that initiates structural failure (Fig. 9 (c)). The critical region that has the largest variation along the pipe axis is

between 0.60*L* and 0.80*L*, matching well with the location of inward bulge in the test. Most of the strains that were measured from test (point A, 05D, and 1D) lie on or close to the predictions curves, as seen in Fig. 9 (c). However, an exception of strain distribution happened in point A, which locates in the central cross-section of the pipe. Such discrepancy may be introduced by the use of the symmetrical boundary condition during simulation. For the hoop strain $\varepsilon_{22}$, as shown in Fig. 9 (d), it starts with a small tension value on point *C* in the beginning stages, and then turns to a large compression value from the lateral region (0.2*L*) all the way to the bottom (0.5*L*), where *L* is the circumference length of the pipe cross-section. This phenomenon demonstrates that the ovalization largely increases in such regions.
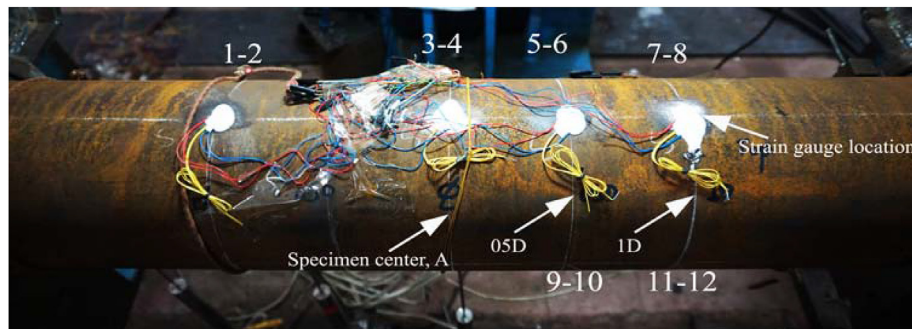


**Fig. 10.** Strain gauge distribution on intact specimen in the test (Point A is the center of the specimen).

### 4.3. Moment-curvature diagrams

The comparison of bending moment-curvature diagrams between test data and numerical predictions is presented in Figs. 11 and 12, which shows a good agreement. Only small scatters happen in the hardening and post-buckling stages. As observed in Fig. 11, there is a slight recovery in terms of the bending moment in the test. This is due to the instability of the real support boundary conditions when the specimen suffers from large curvature. Such system error has been detailed discussed in the former work about the test by Cai et al. (2017b). Instead, there is no such recovery in the simulation results due to its boundary stability. Three dented specimens including S2N1, S2N2 and S2N5 have a dent in $90^o$ on the compression side, whereas specimen S2N3 has a dent in $45^o$. The occurrence of dent has changed the variation tendency of the bending moment-curvature diagram, initiating a rapid failure of specimen and considerably reducing the critical bending curvature. Compared with the intact specimens, $M_{cr}$ decreases by 5%–10% due to the occurrence of a dent.

Tables 2 and 3 list all the comparison results in terms of bending capacity ($M_{cr}$) and critical curvature ($\kappa_{cr}$). For the prediction result of $M_{cr}$, less than 2.25% discrepancy has been obtained for the intact specimen, while less than 3.75% discrepancy has been observed for the damaged specimen. The discrepancy of $\kappa_{cr}$ is less than 2.95% for intact specimen, whereas the prediction results for the damaged specimens presents a relative large scatter. The discrepancies may be introduced by the discrepancies in material properties, the measurement method for the curvature, etc, as discussed in the experimental investigation part of Cai et al. (2017b).

The elastic-plastic failure pattern is dominant with a smooth failure procedure. For an intact specimen, $M_{cr}$ is larger than 1.32 times of $M_y$, while for the damaged specimen, $M_{cr}$ is more than 1.12 times of $M_y$ based on the simulation predictions. It is found that the occurrence of a dent on the compression side reduces the bending capacity of specimen $M_{cr}$ and $\kappa_{cr}$ by at least 8.62% and 60.85%, respectively, compared with the intact specimen S1N4.

## 5. Parametric investigation

Based on the comparison between the simulation results and the test data in the previous section, sufficient confidence has been gained to use the developed numerical models for further investigation. Therefore, the investigation of several parameters that could affect the structural behavior of specimens will be conducted in this section.

### 5.1. Anisotropy effect

As indicated from the material tensile tests in experimental investigation of Cai et al. (2017b), anisotropy in terms of different material yield stress in hoop and longitudinal direction of specimen has

been observed. It may be induced by the manufacturing workmanship of the pipes, such as the thermo-mechanical rolling. In spite of a slight anisotropy of seamless pipe compared with the welded-pipe, such effect is investigated in this section. The Hill48 yield criterion (Hill, 1948) is deployed to take into account the anisotropy feature in numerical simulation. In this place, the material yield stress in the pipe hoop direction varies when the stress keeps constant in the pipe longitudinal direction. As seen in Fig. 13 (a), the effect of anisotropy on such relative thick pipe is insignificant. The results imply that the yield stress in the pipe longitudinal direction dominates the pipe strength.

### 5.2. Initial imperfection effect

The initial imperfection in terms of a wave-type (Fig. 5) is investigated. The comparison results are shown in Fig. 13 (b) and (d). Six types of initial imperfection with different imperfection amplitude-to-thickness ratios are accounted for. The variation of amplitude lies between 3%t-15%t ($t$ is the pipe thickness, the variation range is based on research from Es et al. (2016).), while the specific shape of imperfection is from the eigenvalue buckling analysis of the same model under unit bending moment. The combination of the first two-order eigenvalue shape is used. Both the intact specimen S1N4 and dented specimen S2N1 are adopted with the same friction coefficient and material property (L7) in each case. A very interesting phenomenon has been observed from the simulation results. It can be seen that the initial imperfection has a negative effect on both bending strength and curvature of a pipe without damage, whereas it can hardly affect the structural strength of a dented pipe. Moreover, such effect is still small for an intact specimen, when the imperfection is no larger than 0.06t. A much larger effect happens when the imperfection is larger than 0.11t. For instance, for the case with imperfection of 0.15t, the decrease of critical curvature reaches by 17% compared with the perfect case. Therefore, it can be briefly concluded that the effect of manufacturing induced initial imperfection is insignificant and can be neglected in the FEM simulation for a pipe with a considerable dent size.

### 5.3. Friction effect

The friction of test set-up between the strip and the specimen may affect the strength behavior and corresponding curvature variation. Therefore, an investigation of the friction effect has been carried out with the variation of friction coefficient between 0 and 0.9. As seen in Fig. 13 (c), the introduction of friction results in a considerable variation of the moment-curvature diagram compared with the friction free case. However, the effect is small when the friction coefficient lies in the normal engineering domain, say 0.2–0.4. Then, a significant effect has been observed with the further increase of friction coefficients. For instance, the decrease of critical curvature reaches as large as 30.33% compared with the case with 0.26 friction, and the decrease of bending
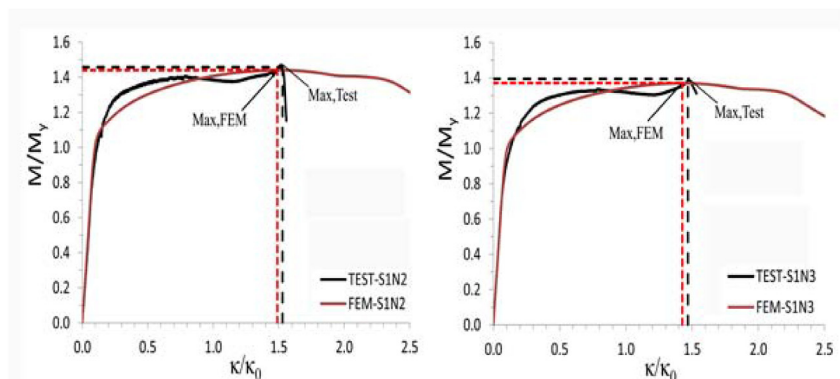


**Fig. 11.** Comparison between numerical and test results in terms of bending moment-curvature diagram for intact specimens: (a) specimen S1N2; (b) specimen S1N3.
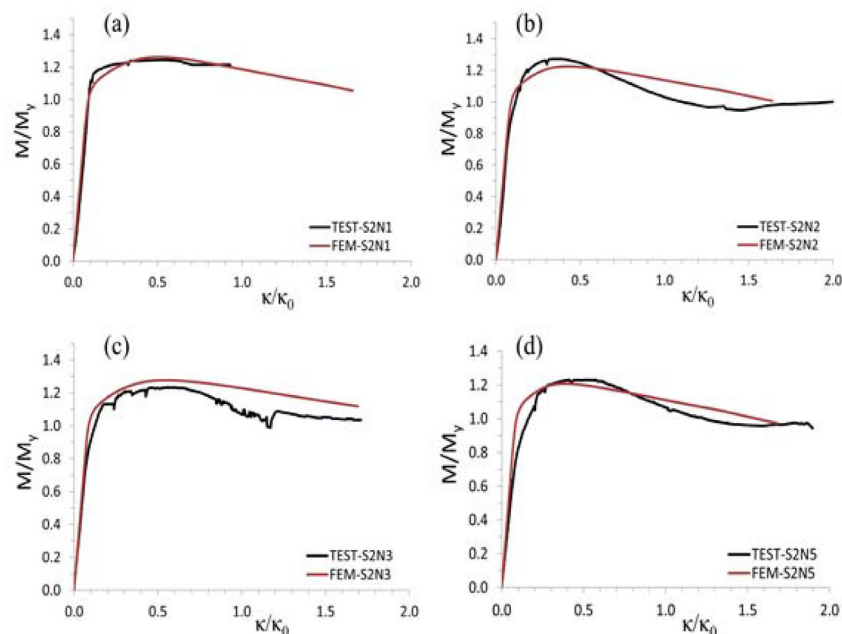
**Fig. 12.** Comparison between numerical and test results in terms of bending moment-curvature diagram for specimens with dent on the compression side: (a) specimen S2N1 with $90^0$ dent; (b) specimen S2N2 with $90^0$ dent; (c) specimen S2N3 with $45^0$ dent; (d) specimen S2N5 with $90^0$ dent.

**Table 2**
The results on intact specimens (dimension unit: mm).

| S·N. | D | t | D/t | $M_{cr}$(Test) | $M_{cr}$(FEA) | $\kappa_{cr}$ (Test) | $\kappa_{cr}$(FEA) |
|------|------|------|-------|------|------|-------|-------|
| | | | | (kNm) | (kNm) | (1/m) | (1/m) |
| S1N1 | 168.09 | 7.90 | 21.28 | 104.37 | 103.39 | 0.422 | 0.421 |
| S1N2 | 167.36 | 7.87 | 21.27 | 103.65 | 102.43 | 0.439 | 0.428 |
| S1N3 | 167.55 | 7.92 | 21.16 | 103.21 | 101.35 | 0.441 | 0.428 |
| S1N4 | 167.01 | 7.84 | 21.30 | 102.71 | 100.40 | 0.401 | 0.412 |

moment has also reached by 5.22%. The reason can be explained as follows: an equivalent axial compression force has been introduced by the loading heads with the increase of rotational angle of the specimen during the quasi-static loading procedure, as seen in Fig. 1 (a). Under a center range, the axial force is small and can be counterbalanced by the friction force. Hence, the structure stays stable. The friction force helps to maintain such stability to some extent. Therefore, the larger the friction force is, the larger the introduced equivalent axial force the test set-up can counterbalance. As a consequence, a lower bending capacity of the specimen is produced due to the effect of such equivalent compression force. It can be concluded that the structural response is quite sensitive to the frictions that have been introduced by the test configuration.

## 6. Simulation results of dent and proposed formulas

A series of numerical simulation are conducted based on the

validated model, changing the geometrical size of dent parameters. The selection of dent follows two aspects. On the one hand, the small dent may not produce significant effect on the structural strength. It is generally accepted by the rules, for instance, the maximum acceptable dent depth is 5%D after impact (DNV, 2013a,b). On the other hand, it is also impractical to account for an extra large dent, which may introduce a rapid failure of the structures in a very short time. Therefore, in this paper, the selected dent depth ($d_d/t$) is between 0.1 and 2.2 (∼ 11%D), while the selected dent length ($\lambda_l$) is between 0.8 and 5.2 (∼ 0.81D). The selected dent width ($\lambda_w = w_d/\sqrt{Rt}$) is between 1.0 and 3.7.

### 6.1. Simulation results of dent

In this section, the effect of a dent on the pipe behavior with respect to dent length ($l_d$), dent depth ($d_d$) and dent width ($w_d$) is investigated based on the developed numerical model (S2N1, 3%t initial imperfection, material L7 (Cai et al., 2017b), anisotropy, central location and compression side, $90^o$ dent). Tables 4–7 list the simulation data. Prediction formulas are then proposed based on these simulation results. The referential values $M_i$ and $\kappa_i$ are 108.9 kNm and 0.367 based on the intact FEM model, respectively. The value of $d_d$ is normalized by the pipe thickness t, while $l_d$ and $w_d$ are normalized by $\sqrt{Rt}$, expressed as $\lambda_l = l_d/\sqrt{Rt}$ and $\lambda_w = w_d/\sqrt{Rt}$, respectively.

Fig. 14 shows the normalized bending moment-curvature diagrams with the variation of the dent depth, length and width. Compared with the intact pipe, it is found that the occurrence of a particular dent affects its strength, Furthermore, as obtained from the former research

**Table 3**
The results of specimens with dent damage (dimension unit: mm; angle unit: degree.

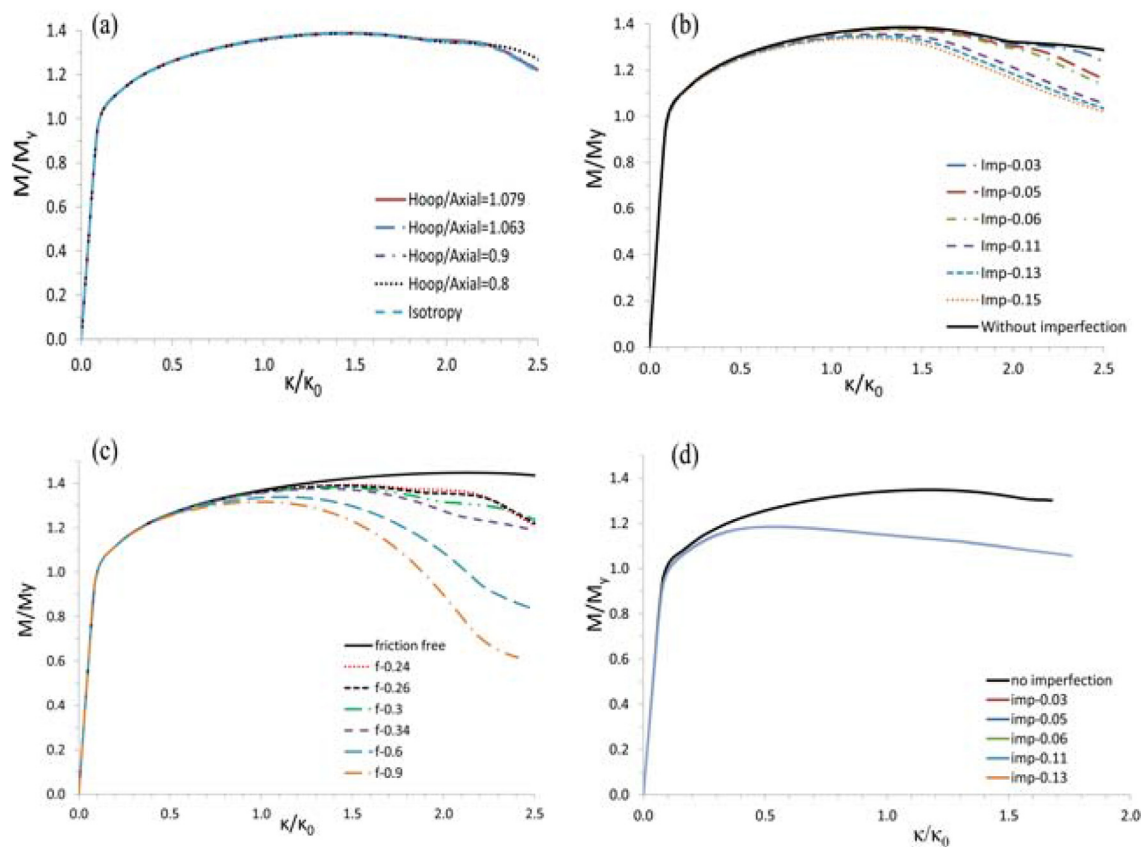| S·N. | D | t | D/t | Dent | Dent | $M_{cr}$(Test) | $M_{cr}$(FEA) | $\kappa_{cr}$(Test) | $\kappa_{cr}$(FEA) |
|------|------|------|-------|------|------|------|------|------|------|
| | | | | ($l_d \times w_d \times d_d$) | angle | (kNm) | (kNm) | (1/m) | (1/m) |
| S2N1 | 169.21 | 8.25 | 20.51 | 89 × 68 × 10.3 | 90 | 92.57 | 93.86 | 0.154 | 0.143 |
| S2N2 | 168.23 | 8.13 | 20.69 | 100 × 75 × 10.3 | 90 | 93.55 | 90.04 | 0.109 | 0.124 |
| S2N3 | 169.38 | 7.90 | 21.44 | 130 × 60 × 10.3 | 45 | 91.65 | 94.83 | 0.158 | 0.157 |
| S2N5 | 168.74 | 8.15 | 20.70 | 110 × 85 × 10.3 | 90 | 90.97 | 89.18 | 0.164 | 0.107 |

**Fig. 13.** Normalized bending moment-curvature diagram with the changing of different parameters: (a) the varying of material anisotropy (based on specimen S1N4); (b) the varying of initial imperfection (based on specimen S1N4); (c) the varying of friction coefficient (based on specimen S1N4); (d) the varying of initial imperfection (based on specimen S2N1).

**Table 4**
Residual ultimate strength of pipes with varying of dent depth.

| Capacity | | | | | $l_d$ = 89 mm, $w_d$ = 68 mm | | | | | | | |
|---|---|---|---|---|---|---|---|---|---|---|---|---|
| | | | | | $d_d/t$ | | | | | | | |
| | 0.12 | 0.36 | 0.48 | 0.61 | 0.73 | 0.85 | 0.97 | 1.25 | 1.33 | 1.45 | 1.58 | 1.70 |
| $M_{cr}/M_i$ | 0.998 | 0.968 | 0.943 | 0.922 | 0.905 | 0.891 | 0.880 | 0.862 | 0.856 | 0.852 | 0.848 | 0.844 |
| $\kappa_{cr}/\kappa_i$ | 1.001 | 0.736 | 0.586 | 0.510 | 0.452 | 0.431 | 0.398 | 0.390 | 0.381 | 0.379 | 0.387 | 0.368 |
| | 1.82 | 1.94 | 2.06 | 2.18 | | | | | | | | |
| $M_{cr}/M_i$ | 0.843 | 0.841 | 0.840 | 0.839 | | | | | | | | |
| $\kappa_{cr}/\kappa_i$ | 0.384 | 0.392 | 0.395 | 0.392 | | | | | | | | |

**Table 5**
Residual ultimate strength of pipes with varying of dent length.

| Capacity | | | | | $d_d$ = 5.3 mm, $w_d$ = 68 mm | | | | | | | |
|---|---|---|---|---|---|---|---|---|---|---|---|---|
| | | | | | $\lambda_l = l_d/\sqrt{Rt}$ | | | | | | | |
| | 0.8 | 1.5 | 2.0 | 2.3 | 2.5 | 3.4 | 4.2 | 4.5 | 4.7 | 5.0 | 5.2 | |
| $M_{cr}/M_i$ | 0.998 | 0.992 | 0.975 | 0.961 | 0.952 | 0.916 | 0.890 | 0.879 | 0.875 | 0.869 | 0.864 | |
| $\kappa_{cr}/\kappa_i$ | 1.011 | 0.978 | 0.771 | 0.689 | 0.638 | 0.488 | 0.401 | 0.381 | 0.354 | 0.349 | 0.360 | |

by Cai et al. (2018a), it is also observed from Fig. 15 that both the dent depth ($d_d$) and length ($l_d$) have a considerable influence on the bending behavior, decreasing both the ultimate bending moment and critical curvature significantly. For instance, a dent length equal to 3.37 times of $\sqrt{Rt}$ can reduce the $M_{cr}$ and $\kappa_{cr}$ by more than 14% and 61%, respectively, and a dent depth equal to 0.73 times of the pipe thickness

($\sim 0.35D$) can reduce the $M_{cr}$ and $\kappa_{cr}$ by more than 9% and 50%, respectively. Meanwhile, the dent width ($w_d$) has a slight effect, as can be seen in Figs. 14 (c) and Fig. 15. Comparing results with the variation of dent width in a large domain show that the variation values are less than 3% and 1% for $M_{cr}$ and $\kappa_{cr}$, respectively. It is plausible to neglect the dent width effect on the structural behavior of such pipes.

**Table 6**
Residual ultimate strength of pipes with varying of dent length.

| Capacity | $d_d = 10.3\,mm$, $w_d = 68\,mm$ | | | | | | | | | | | |
|---|---|---|---|---|---|---|---|---|---|---|---|---|
| | $\lambda_l = l_d/\sqrt{Rt}$ | | | | | | | | | | | |
| | 0.80 | 1.51 | 1.60 | 1.70 | 1.80 | 1.90 | 2.00 | 2.20 | 2.30 | 2.40 | 2.50 | 2.90 |
| $M_{cr}/M_i$ | 0.997 | 0.980 | 0.975 | 0.969 | 0.962 | 0.956 | 0.949 | 0.935 | 0.928 | 0.921 | 0.914 | 0.888 |
| $\kappa_{cr}/\kappa_i$ | 0.980 | 0.888 | 0.845 | 0.785 | 0.741 | 0.703 | 0.670 | 0.586 | 0.567 | 0.520 | 0.501 | 0.436 |
| | 3.37 | 3.79 | 4.16 | 4.54 | 4.70 | 4.80 | 5.00 | 5.10 | 5.20 | | | |
| $M_{cr}/M_i$ | 0.862 | 0.838 | 0.81 | 0.803 | 0.797 | 0.793 | 0.785 | 0.783 | 0.780 | | | |
| $\kappa_{cr}/\kappa_i$ | 0.390 | 0.338 | 0.302 | 0.286 | 0.270 | 0.264 | 0.253 | 0.251 | 0.267 | | | |

**Table 7**
Residual ultimate strength of pipes with varying of dent width.

| Capacity | $d_d = 10.3\,mm$, $l_d = 89\,mm$ | | | | | | | | |
|---|---|---|---|---|---|---|---|---|---|
| | $\lambda_w = w_d/\sqrt{Rt}$ | | | | | | | | |
| | 1.06 | 1.44 | 1.89 | 2.04 | 2.20 | 2.35 | 2.95 | 3.33 | 3.71 |
| $M_{cr}/M_i$ | 0.856 | 0.853 | 0.855 | 0.855 | 0.857 | 0.858 | 0.865 | 0.870 | 0.875 |
| $\kappa_{cr}/\kappa_i$ | 0.395 | 0.381 | 0.376 | 0.371 | 0.379 | 0.384 | 0.390 | 0.395 | 0.403 |
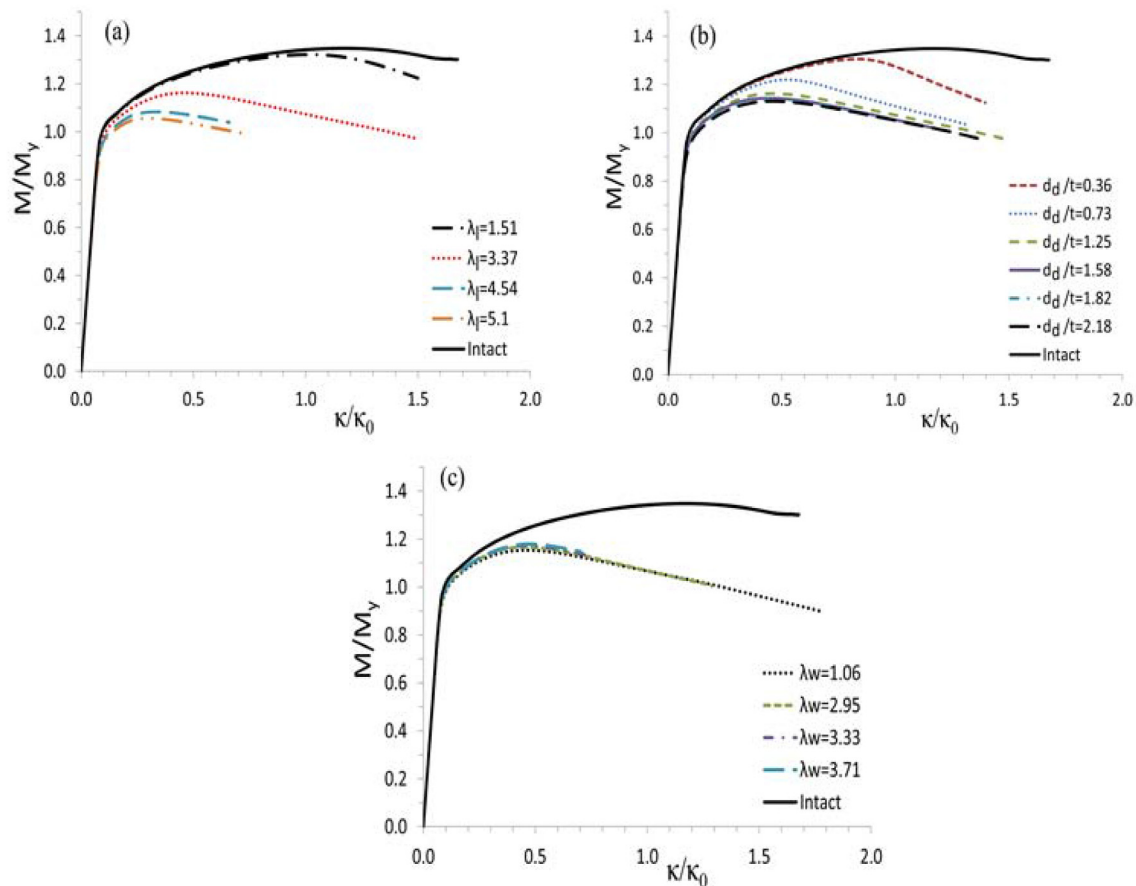


**Fig. 14.** Normalized bending moment-curvature diagrams with varing of dent parameters (S2N1, $90^o$): (a) diagrams with variation of normalized dent length ($\lambda_l$, $d_d = 10.3\,mm$, $w_d = 68\,mm$); (b) diagrams with variation of normalized dent depth ($d_d/t$, $l_d = 89\,mm$, $w_d = 68\,mm$); (c) diagrams with variation of normalized dent width ($\lambda_w$, $l_d = 89\,mm$, $d_d = 10.3\,mm$).

## 6.2. Proposed formulas

Based on the former research and the simulation data, it is reasonable to propose formulas as function of $l_d$ and $d_d$. The formulas are

constructed as follows:

$$M_{cr}/M_i(\kappa_{cr}/\kappa_i) = 1 - f(\lambda_l, d_d/t) \tag{2}$$

where $\lambda_l$ is the normalized dent length in the pipe hoop direction, $M_i$ and $\kappa_i$ are the ultimate bending moment and the critical curvature from
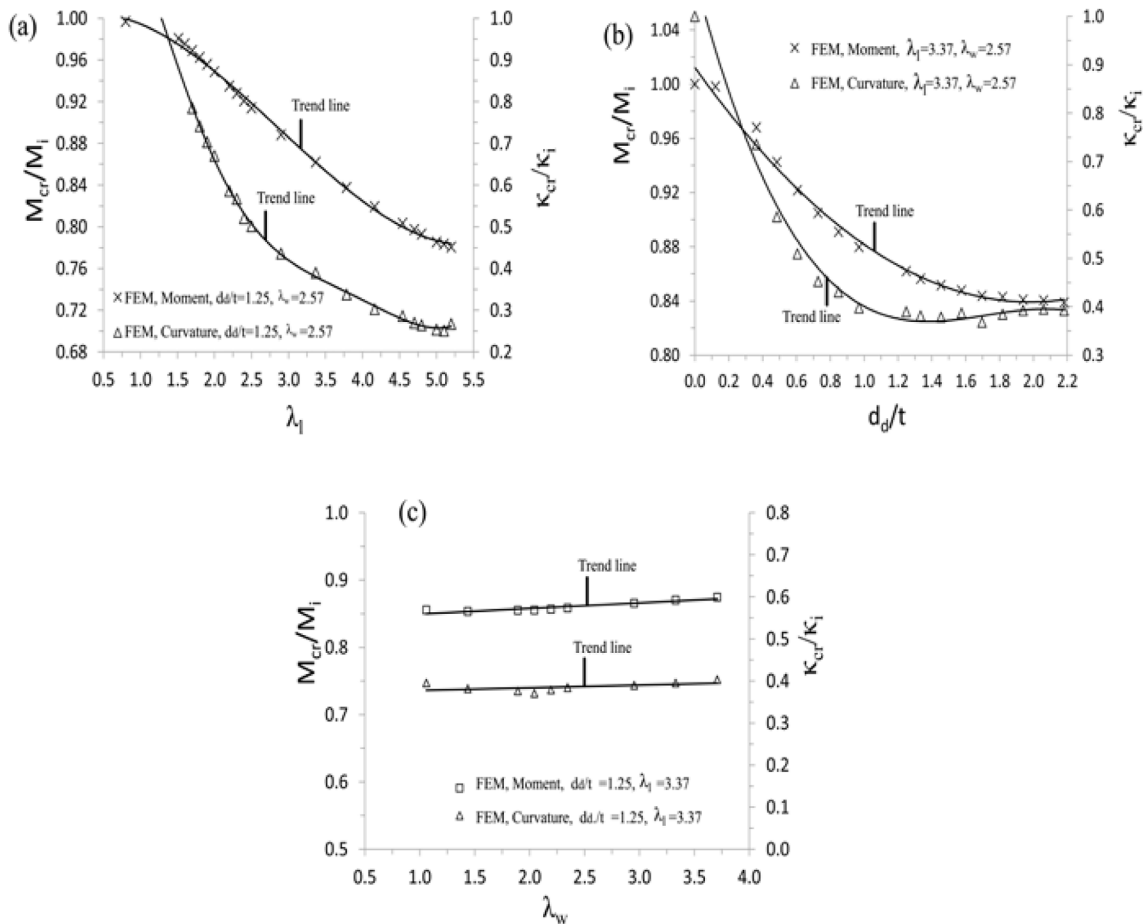
Fig. 15. The effect of dent parameters: (a) dent length; (b) dent depth; (c) dent width.
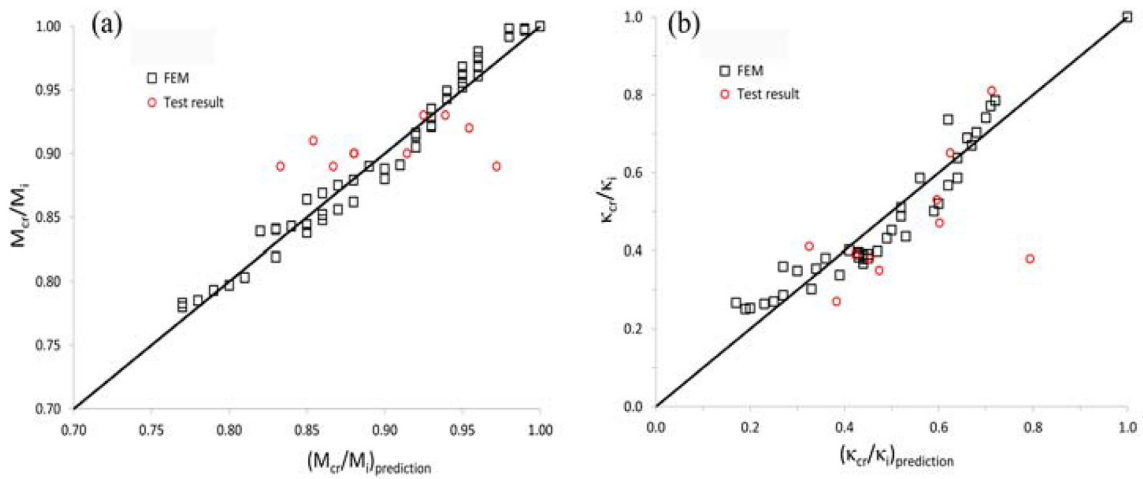


Fig. 16. Comparison between prediction of proposed equations and both experimental and numerical results: (a) normalized residual ultimate moment ($M_{cr}/M_i$); (b) normalized critical curvature ($\kappa_{cr}/\kappa_i$).

**Table 8**
Model uncertainties of the proposed formulas.

| X | Moment, Eq. (3) | COV | Curvature, Eq. (4) | COV |
|---|---|---|---|---|
| | Mean (Bias) | | Mean (Bias) | |
| FEM | 1.0014 | 0.0124 | 1.024 | 0.1541 |
| Test | 1.0068 | 0.0459 | 0.892 | 0.2563 |

the simulation of intact pipes, respectively.

A regression analysis on the FEM results is undertook to build up the relationship between the prediction values and the significant dent parameters.

$$M_{cr}/M_i = 1 - a_1(d_d/t)^{b_1}(\lambda_l)^{c_1} \tag{3}$$

$$\kappa_{cr}/\kappa_i = 1 - (a_2 + b_2 t/d_d)(\lambda_l)^{c_2} \tag{4}$$

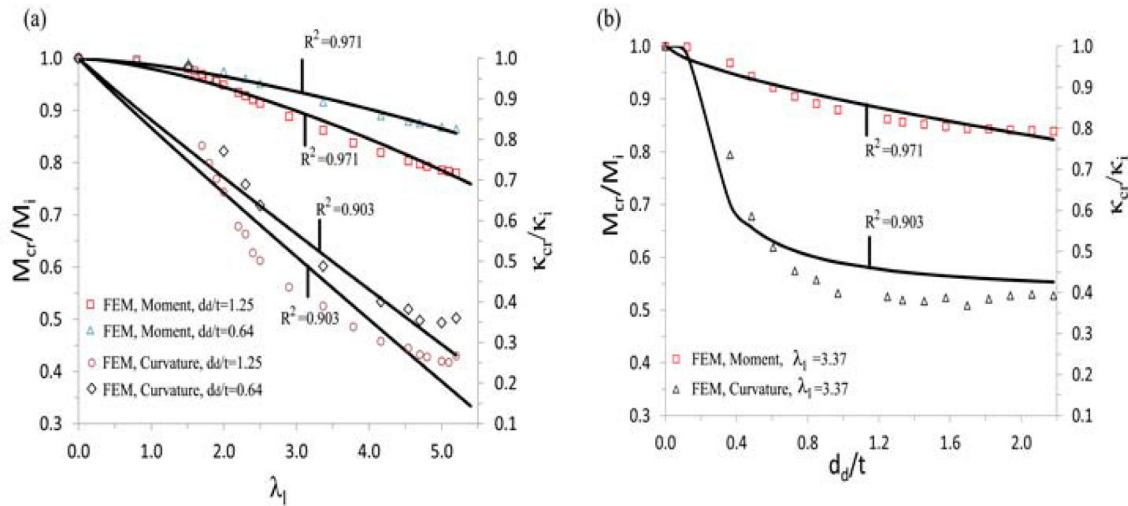Where $a_1$, $b_1$ and $c_1$ is 0.017, 0.696 and 1.48, respectively; $a_2$, $b_2$ and

**Fig. 17.** Prediction of dented metallic pipes with the changing of dent parameters: (a) variation of normalized dent length ($\lambda_l = l_d/\sqrt{Rt}$); (b) variation of normalized dent depth ($d_d/t$).

$c_2$ is 0.192, −0.026 and 0.955, respectively.

In order to validate the accuracy of the proposed formulas, the prediction results are compared with both the test and simulation results, as shown in Fig. 16. It shows that the two proposed equations have a satisfying comparison with the simulation results. Compared with the test results, the formula has a little pessimistic estimation for some cases, which is probably due to the discrepancies in test such as material, and geometry measurement. Furthermore, following the definition from Bai et al. (1994), the model uncertainty parameter can be written as:

$$X = X_{true}/X_{predict} \tag{5}$$

Where $X_{true}$ is the data from either experimental test or numerical simulation, and $X_{predict}$ is the prediction values due to the proposed equations. It is assumed that both $X_{true}$ and $X_{predict}$ are from the same cases with the same material properties and geometry. Hence, the mean value (bias), standard error of X, and the coefficient of variation (COV) are statistically calculated, as shown in Table 8.

The model uncertainties of the proposed equations indicate that the extent of variability for the prediction of residual bending moment is smaller than 5% in relation to the mean bias value. For the critical curvature, the equation provides a predcition with a relative large scatter, as seen from the mean bias value of 0.892 and the COV of 0.2563 from the comparison with test data.

Fig. 17 shows the prediction results of dented metallic pipes with the changing of dent parameters. Two different dent depth including $d_d/t = 1.25$ and $d_d/t = 0.64$ are used when the normalized dent length is varying (Fig. 17 (a)), while the normalized dent length is fixed to $\lambda_l = 3.37$ when the dent depth is varying (Fig. 17 (b)). The FEM results are also presented in these figures. The R square of the fitted equation are 0.971 and 0.903, respectively, which reflects a higher precision of prediction.

In practice, the proposed equations can be used when a dent is produced due to a sudden mechanical interference such as the impact between fishing boat and pipes, and the dropping of foreign objects. Only a simple measurement of the damage length and depth is needed to estimate the reduction ratio of pipe strength under dominated bending moment. It should be noted that, the length of dent should be projected to the hoop direction of pipe if there is a rotational angle on the dent. The impact induced residual stress has not been accounted for in these equations due to the lack of test data. Further extensions of the application domain on pipes with different $D/t$ and different materials are needed.

## 7. Conclusions

On the basis of an experimental investigation, this paper has provided an extensive numerical investigation on seamless pipes with low diameter-to-thickness ratio that suffered from dent damage. Numerical models accounting for the structural damage have been developed, which can provide a parametric modeling tool based on the nonlinear FEM. Based on the numerical models, an investigation of influential parameters has been conducted. The conclusions of this paper are as follows:

1. The developed numerical models are capable of providing a reasonable prediction on the bending behavior in terms of bending moment, critical curvature and failure mode.
2. The occurrence of a dent damage accelerates the failure of pipe due to the rapid localization of the damaged region with an elastic-plastic failure mode.
3. The material yield stress in the pipe longitudinal direction dominates the bending capacity of the structures. For a pipe with a considerable dent size, the effect of manufacturing induced initial imperfection is insignificant.
4. The dent length ($l_d$) and depth ($d_d$) have significant effects on the pipe strength, whereas the dent width ($w_d$) only slightly affects the strength.
5. Based on the FEM results, empirical formulas are proposed to predict the residual ultimate strength of metallic pipes in terms of bending moment ($M_{cr}$) and critical curvature ($\kappa_{cr}$) under pure bending moment. These formulas could be utilized for practice purposes to estimate the residual bending strength of pipes after the suffering of dent damage.

## References

Abaqus6.13, 2013. Abaqus: User's Manual. 6.13.
Bai, Q., Bai, Y., 2014a. Subsea Pipeline Design, Analysis, and Installation. Gulf

Professional Publishing.

Bai, Y., Bai, Q., 2014b. Subsea Pipeline Integrity and Risk Management. Gulf Professional Publishing.

Bai, Y., Igland, R.T., Moan, T., 1994. Ultimate limit states of pipes under tension and bending. Int. J. Offshore Polar Eng. 4 (04) 1994.

Bjørnøy, O., Rengård, O., Fredheim, S., Bruce, P., 2000. Residual strength of dented pipelines, DNV test results. In: The Tenth International Offshore and Polar Engineering Conference. International Society of Offshore and Polar Engineers.

Cai, J., Jiang, X., Lodewijks, G., 2017a. Residual ultimate strength of offshore metallic pipelines with structural damage–a literature review. Ships Offshore Struct. 1–19.

Cai, J., Jiang, X., Lodewijks, G., 2018a. Numerical investigation of residual ultimate strength of dented metallic pipes subjected to pure bending. Ships Offshore Struct. 13 (5).

Cai, J., Jiang, X., Lodewijks, G., Pei, Z., Wu, W., 2018b. Residual ultimate strength of damaged seamless metallic pipelines with combined dent and metal loss (accepted). Mar. Struct. 61, 188–201.

Cai, J., Jiang, X., Lodewijks, G., Pei, Z., Wu, W., 2018c. Residual ultimate strength of damaged seamless metallic pipelines with metal loss. Mar. Struct. 58, 242–253.

Cai, J., Jiang, X., Lodewijks, G., Pei, Z., Zhu, L., 2017b. Experimental investigation of residual ultimate strength of damaged metallic pipelines. In: ASME 2017 36th International Conference on Offshore Mechanics and Arctic Engineering. American Society of Mechanical Engineers.

Cai, J., Jiang, X., Lodewijks, G., et al., 2016. Residual strength of metallic pipelines subject to combined loads accounting for impact induced damage. In: The 26th International Ocean and Polar Engineering Conference. International Society of Offshore and Polar Engineers.

DNV, 2010. DNV-RP-F111:Interference between Trawl Gear and Pipelines. Det Norske Veritas. latest Edition.

DNV, 2013a. DNV-OS-F101 Submarine Pipeline Systems. Det Norske Veritas.

DNV, 2013b. DNV-RP-C208: Determination of Structural Capacity by Non-linear FE Analysis Methods. Det Norske Veritas.

Es, S., Gresnigt, A., Vasilikis, D., Karamanos, S., 2016. Ultimate bending capacity of spiral–welded steel tubes–part i: Experiments. Thin-Walled Struct. 102, 286–304.

GB/T 1591, 2008. High Strength Low alloy Structural Steels (In Chinese). The Chinese National Standard. latest Edition).

Gellin, S., 1980. The plastic buckling of long cylindrical shells under pure bending. Int. J. Solid Struct. 16 (5), 397–407.

Ghaednia, H., SreekantaDas, Wang, RichardKania, R., 2015. Safe burst strength of a

pipeline with dent–crack defect: effect of crack depth and operating pressure. Eng. Fail. Anal. 55, 288–299.

Gresnigt, A., Van Foeken, R., 2001. Local buckling of UOE and seamless steel pipes. In: The Eleventh International Offshore and Polar Engineering Conference. International Society of Offshore and Polar Engineers.

Guarracino, F., Walker, A., Giordano, A., 2009. Effects of boundary conditions on testing of pipes and finite element modelling. Int. J. Pres. Ves. Pip. 86 (2), 196–206.

Hilberink, A., 2011. Mechanical Behaviour of Lined Pipe. PhD Thesis. Delft University of Technology.

Hill, R., 1948. A theory of the yielding and plastic flow of anisotropic metals. Proceedings of the Royal Society A 193.

Jones, N., Kitching, R., 1966. An experimental investigation of a right-angled single unreinforced mitred-bend subjected to various bending moments. J. Strain Anal. 1 (3), 248–263.

Macdonald, K., Cosham, A., 2005. Best practice for the assessment of defects in pipelines–gouges and dents. Eng. Fail. Anal. 12 (5), 720–745.

Murphey, C., Langner, C., 1985. Ultimate pipe strength under bending, collapse and fatigue. In: Proceedings of the 4th International Conference on Offshore Mechanics and Arctic Engineering. vol. 1. pp. 467–477.

Park, T., Kyriakides, S., 1996. On the collapse of dented cylinders under external pressure. Int. J. Mech. Sci. 38 (5), 557–578.

PHMSA, 2017. Pipeline Incident 20 Year Trend. Tech. Rep. U.S.Department of Transportation.

Prabu, B., Raviprakash, A., Venkatraman, A., 2010. Parametric study on buckling behaviour of dented short carbon steel cylindrical shell subjected to uniform axial compression. Thin-Walled Struct. 48 (8), 639–649.

Sherman, D.R., 1976. Test of circular steel tubes in bending. J. Struct. Div. 102 (11), 2181–2195.

Vasilikis, D., Karamanos, S.A., van Es, S.H., Gresnigt, A.M., 2016. Ultimate bending capacity of spiral-welded steel tubes–part ii: Predictions. Thin-Walled Struct. 102, 305–319.

Vitali, L., Bartolini, L., Askheim, D., Peek, R., Levold, E., 2005. Experimental test and FE analyses. In: ASME 2005 24th International Conference on Offshore Mechanics and Arctic Engineering. American Society of Mechanical Engineers, pp. 715–729 Hotpipe JI project.

Weiner, P., Smith, S., 1976. Maximum moment capability of pipe with various d/t ratios. Journal of Engineering for Industry 98 (3), 1107–1111.